A Solution of Coplanar Waveguide with Air-bridges Using Complex Images

Amjad A. Omar and Y. Leonard Chow, *Member, IEEE*

Abstract—**A new method is proposed to solve general CPW circuits including air-bridges. This method generalizes the integral equation technique to nonplanar structures containing hybrid electric and magnetic currents. It also exploits the full wave *complex image technique* to efficiently calculate the Green's functions of this structure. The proposed method, therefore, offers a substantial reduction in computer time and memory over many other full wave methods. The accuracy of the proposed method is checked by comparing with available FDTD-theoretical and experimental results for a CPW band reject filter. Using only 92 matching points, our method gave very good agreement.**

I. Introduction

During the past few years, there has been a growing interest in coplanar waveguides (CPWs) as transmission lines suitable for microwave and millimeter wave frequencies. This is due to the appealing properties of CPWs such as: 1) In CPWs there is no need to drill via holes for grounding purposes and for shunt connections as in microstriplines [1]. 2) In CPWs there is no need to build excessively thin, and therefore fragile, substrates to get a higher characteristic impedance (Z_o). The reason for this is that Z_o in CPW can be adjusted by changing the slot to strip width ratio without having to change the substrate thickness [2].

However, the main disadvantages of CPWs are: 1) The excitation of the parasitic coupled (odd) slotline mode by the nonsymmetric CPW discontinuities like bends and T-junctions [3]. This mode propagates at a different velocity from the dominant even CPW mode and causes more radiation to free space. 2) The lack of theoretical investigation of many CPW circuits.

A number of researchers studied the CPW discontinuities, like end effects [4]–[6], T-junctions [7], etc. They, also, used air-bridges to equate the potentials of the two ground planes and thus eliminate the coupled slotline mode.

Several methods were recently applied to the solution of CPW circuits with air-bridges. Dib *et al.* [8] and Bromme *et al.* [9] used a hybrid technique for solving this problem. In this technique the 2N port representation of the odd and even modes of the CPW circuit without air-bridges is first obtained using the full wave analysis. Then the air-bridges are included in this representation in the form of their quasi-static models.

The only published full wave analysis results on the air-bridges were reported by Rittweger *et al.* [10] and Beilenhoff *et al.* [11]. Rittweger [10] used the FDTD method to solve for the S-parameters of a CPW band reject filter with and without air-bridges. Beilenhoff [11] used the three dimensional finite difference method in the frequency domain to solve for the scattering behavior of the air-bridges. However, these full wave methods require a large computer storage capability and are computationally inefficient.

In this paper, we present an accurate and computationally efficient full wave method for solving general CPW circuits including the air-bridges. This method uses the full wave mixed potential integral equation technique [12] combined with the moment method [13] to solve this problem. This technique was reported in the literature to solve planar structures containing hybrid electric and magnetic currents [14]. However, in this paper, it is extended to the solution of the planar CPW circuit with the vertical air-bridges, carrying hybrid currents.

The full wave Green's functions for this structure are obtained using the *complex image technique* [15], which avoids the time consuming numerical integration of Sommerfeld integrals and yields a highly convergent set of images. This set consists of real images which represent the low frequency solution and are dominant in the near field, complex images which include the radiation effect, and finally the surface wave contribution which is dominant in the far field. This will be explained in detail in Section II-C.

To check the accuracy of the proposed method, it is applied to study the behavior of a CPW band reject filter with and without air-bridges. The results obtained are then compared with published experimental and theoretical results on this filter. Very good agreement is obtained over the whole frequency range investigated as will be shown in Section III.

The theoretical Section II consists of two main parts: The first part excludes the air-bridges. It explains the formulation of the mixed potential integral equation for CPW (MPIE), the moment method solution to this MPIE and the final expressions for the complex image Green's func-

Manuscript received December 9, 1991; revised April 2, 1992. This work was supported by funds from the NSERC (National Science and Engineering Research Council) ITRC (Information Technology Research Center) and the University of Waterloo.

The authors are with the Department of Electrical and Computer Engineering, University of Waterloo, Waterloo, ON, Canada N2L 3G1.

IEEE Log Number 9202901.

tions. The second part includes the air-bridges by modifying the MPIE into a pair of coupled MPIE's. In Section III, numerical results for the S-parameters of the band reject filter are shown as compared to previously published experimental and theoretical results.

II. Theoretical Formulation

A. Duality Formulation for Converting the CPW into Parallel Strips

We now formulate the open (i.e. nonshielded) CPW problem of Fig. 1, where it is assumed that the center strip and the ground planes are infinitely thin perfect conductors and that the dielectric is lossless. This problem is solved using the mixed potential integral equation technique [12].

The CPW has two slots. Therefore, similar to a slot antenna, the two slots and the ground plane can be transformed into two equivalent strips without ground plane through the *duality principle* [16]. However, because of the dielectric substrate, the duality principle has to be applied separately for the upper and lower half spaces as shown in Fig. 2(a)–(c).

For the upper half space with no dielectric slab, the transformation by duality is the usual one resulting in an equivalent full space parallel strips problem of Fig. 2(b). For the lower half space with a dielectric slab, the transformation results in the full space problem of parallel strips embedded inside a magnetic slab (characterized by ϵ_o, $\mu_r\mu_o$ with $\mu_r = \epsilon_r$) of Fig. 2(c).

On the strip boundaries: 1) The tangential magnetic fields of the upper and lower subproblems are continuous. Therefore, the (equivalent) electric current density on the strips in the upper subproblem must be equal and opposite to the (equivalent) electric current density in the lower subproblem. 2) The tangential electric fields in both subproblems are continuous. Since each subproblem occupies only a half space, the two conditions above imply:

$$\tfrac{1}{2}\{\hat{n}_s \times [\vec{E}_1(\vec{J}_s) - \vec{E}_2(-\vec{J}_s)]\} = -\hat{n}_s \times \vec{E}^i \quad \text{on the parallel strips.} \tag{1}$$

Where the half factor is due to the contribution of a half space. $\vec{E}_1$, $\vec{E}_2$ are the electric fields on the strips of the upper and lower subproblems, respectively, due to the electric currents on these strips. $\vec{E}^i$ is the impressed $\vec{E}$-field. $\hat{n}_s$ is a unit vector normal to the strips.

The MPIE resulting from (1) is given by

$$\tfrac{1}{2}\left\{\hat{n}_s \times \left[j\omega \iint_{S_{strips}} \left(\overline{\overline{G}}_A^{(1)} + \overline{\overline{G}}_A^{(2)}\right) \cdot \vec{J}_s(\vec{r}\,')\, dS' + \nabla \iint_{S_{strips}} (G_q^{(1)} + G_q^{(2)})\, \rho(\vec{r}\,')\, dS' \right]\right\} = \hat{n}_s \times \vec{E}^i \tag{2}$$

where $\overline{\overline{G}}_A^{(1)}$, $\overline{\overline{G}}_A^{(2)}$ are the dyadic Green's functions for the magnetic vector potentials in the upper and lower subproblems, respectively. $G_q^{(1)}$, $G_q^{(2)}$ are the Green's functions for the electric potential of a single point charge (ρ) in the upper and lower subproblems, respectively. This charge density $\rho(\vec{r}\,')$ is related to the current density $\vec{J}_s(\vec{r}\,')$ by the continuity equation. These Green's functions are explained in Section II-C.

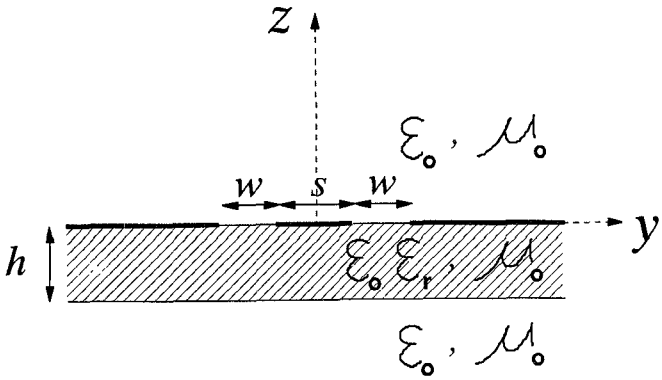

Fig. 1. The cross section of a coplanar waveguide.

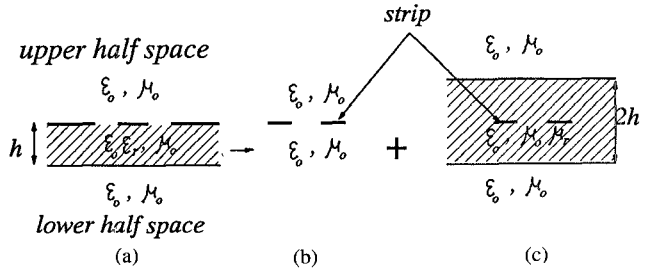

Fig. 2. Splitting the CPW problem (without air-bridges) into two parallel strips subproblems through duality: (a) The original CPW problem. (b) The upper subproblem in free space. (c) The lower subproblem in a magnetic slab with $\mu_r = \epsilon_r$.

B. The Moment Method Solution of the MPIE for the Parallel Strips

Following Harrington [13], the 3-D moment method is used to solve for the unknown current density ($\vec{J}_s$) on the finite length parallel strips as shown in Fig. 3. Therefore, $\vec{J}_s$ and ρ in (2) are expanded in terms of a finite number of pulse basis functions along the strips and satisfy the edge condition across the strips [17]. These basis functions were found to give accurate and highly convergent results for microstriplines [18]. In addition, it is assumed that $\vec{J}_s$ has a negligible transverse component. This assumption was found to be valid for thin strips whose width does not exceed $\lambda_g/20$ [18]. This assumption significantly reduces the computations.

After expanding $\vec{J}_s$ in (2), Galerkin's procedure is used to minimize the error. Thus, the original MPIE reduces to the following matrix equation:

$$\tfrac{1}{2}\{[Z_1] + [Z_2]\}\, \underline{I}^e = \underline{V}^e \tag{3}$$

where $\underline{I}^e$ is the vector of unknown electric (not magnetic) current on the parallel strips. $\underline{V}^e$ is the vector of known electric voltage excitation on the parallel strips and is shown in Fig. 3, where the voltage polarity in this figure

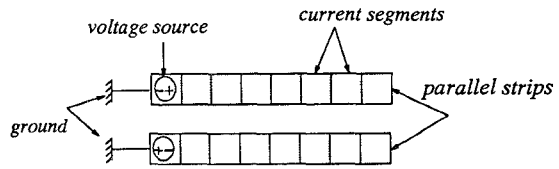

Fig. 3. The voltage source locations on the parallel strips.

will excite the dominant even CPW mode. In addition, the grounding connections in Fig. 3 are achieved by deleting the end charges of the grounded segments [19]. $[Z_1]$, $[Z_2]$ are the impedance matrices for the upper and lower subproblems, respectively. In the evaluation of these impedance matrices, the *multi-pipe* technique [20] is used to insure the rapid convergence of the edge singularities of the charge and current distributions as well as the singularities in the Green's functions.

After solving (3), the obtained current on the strips ($\underline{I}^e$) is used to calculate the scattering parameters of the dual parallel strips problem following an accurate deembedding technique proposed by Mosig [12]. The scattering parameters of the dual strips problem are the same as those of the original CPW problem.

C. The Spatial Green's Functions

For the upper subproblem in free space, in 3-D with cross section as shown in Fig. 2(b), the spatial Green's functions $G_{A_{xx}}^{(1)}$ and $G_q^{(1)}$ are simply the free space Green's functions. However, for the lower subproblem in an inhomogeneous space, with cross section as shown in Fig. 2(c), the full wave spatial (3-D) Green's functions $G_{A_{xx}}^{(2)}$ and $G_q^{(2)}$ are obtained using the *complex image technique* [15]. Because of space limitations and the fact that the technique is well known, this paper only provides the final expressions of these Green's functions. The derivations and the complete expressions are found in [21].

The duality principle of CPW from Fig. 1 to Fig. 2 indicates that for the lower subproblem in Fig. 2(c), the Green's functions need only be evaluated with the source and field points both located in the center plane between the magnetic slab surfaces. Fig. 2(c) is redrawn in Fig. 4 to indicate the coordinate system and the fact that only horizontal dipoles are required for CPW.

For a horizontal (x-directed) 3-D electric current dipole of unit strength embedded in a magnetic slab, the spatial Green's functions can be represented as follows [21]:

$$G_{A_{xx}}^{(2)} = G_{A_{xx_o}}^{(2)} + G_{A,sw}^{xx} + G_{A,ci}^{xx} \tag{4}$$

$$G_q^{(2)} = G_{qo}^{(2)} + G_{q,sw} + G_{q,ci} \tag{5}$$

where $G_{A_{xx}}^{(2)}$ is the x-directed magnetic vector potential due to an x-directed electric current dipole. $G_q^{(2)}$ is the scalar potential associated with one charge of the dipole. In particular, $G_{A_{xx_o}}^{(2)}$ contains the contributions of the source term and the quasi-dynamic [22] current images resulting from the magnetic slab surfaces as shown in Fig. 5. $G_{qo}^{(2)}$ contains the contribution of the source term only since there are no quasi-dynamic charge images in the magnetic slab

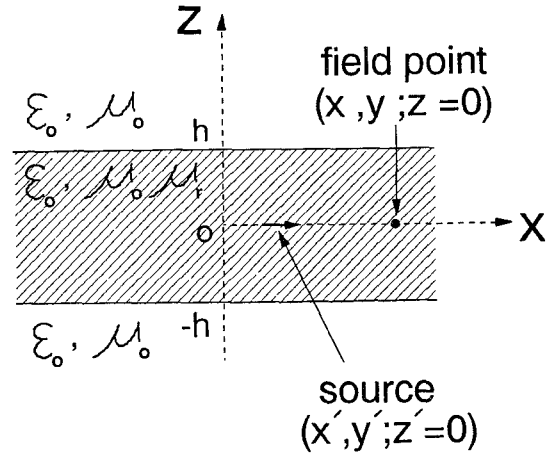

Fig. 4. A horizontal current dipole embedded inside a magnetic substrate (characterized by ϵ_o, $\mu_r\mu_o$).

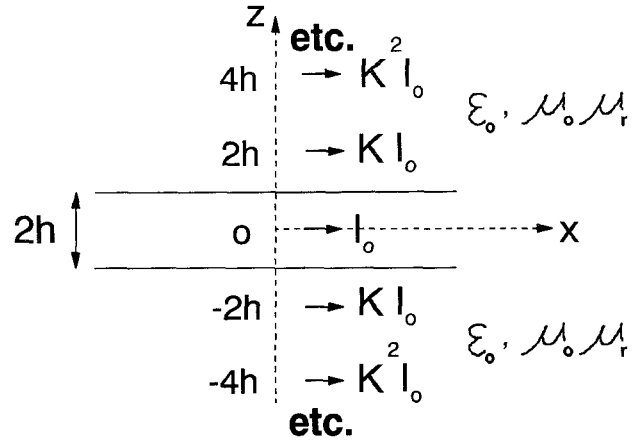

Fig. 5. The quasi-dynamic current images for the lower subproblem of Fig. 2(c) for the fields inside the substrate ($K = (1 - \mu_r)/(1 + \mu_r)$).

of Fig. 4. The quasi-dynamic contributions are dominant in the near field. $G_{A,sw}^{xx}$, $G_{q,sw}$ are the surface wave contributions which are dominant in the far field. They are given by

$$G_{A,sw}^{xx} = \frac{\mu_o\mu_r}{4\pi}(-2\pi j)\ \mathrm{Res}_1\ H_o^2(k_{\rho p}\rho)k_{\rho p} \tag{6}$$

$$G_{q,sw} = \frac{1}{4\pi\epsilon_o}(-2\pi j)\ \mathrm{Res}_2\ H_o^2(k_{\rho p}\rho)k_{\rho p} \tag{7}$$

where $k_{\rho p}$ is the pole location, and the residues Res_1, Res_2 are given in [21]. Finally, dominating in the intermediate field, the last terms of (4) and (5), $G_{A,ci}^{xx}$ and $G_{q,ci}$, are given by

$$G_{A,ci}^{xx} = \frac{\mu_o\mu_r}{4\pi}\int_{-\infty}^{\infty}\frac{1}{j2k_{z_1}}F_1(k_{z_1})H_o^{(2)}(k_\rho\rho)k_\rho\,dk_\rho \tag{8}$$

$$G_{q,ci} = \frac{1}{4\pi\epsilon_o}\int_{-\infty}^{\infty}\frac{1}{j2k_{z_1}}F_2(k_{z_1})H_o^{(2)}(k_\rho\rho)k_\rho\,dk_\rho \tag{9}$$

where the functions $F_1(k_{z_1})$ and $F_2(k_{z_1})$ in (8), (9) are given in [21].

Following [15], each of the functions F_1 and F_2 can be expanded in terms of a sum of exponentials using

Prony's method [23]. The general form of this sum is $\Sigma_{i=1}^{N} a_i e^{jb_i k_{z_1}}$, where a_i's and b_i's are both complex. Then, Sommerfeld's identity [24] is used to perform the integrations in (8) and (9) analytically. This results in the Green's functions of (10) and (11), which may be identified to be those from a set of *complex images* having complex amplitudes (a_i and a_i', respectively) and complex locations ($z' - jb_i$ and $z' - jb_i'$, respectively). i.e.

$$G_{A,ci}^{xx} = \frac{\mu_r \mu_o}{4\pi} \sum_{i=1}^{N} a_i \frac{e^{-jkr_i}}{r_i} \tag{10}$$

$$G_{q,ci} = \frac{1}{4\pi\epsilon_o} \sum_{i=1}^{N} a_i' \frac{e^{-jkr_i'}}{r_i'} \tag{11}$$

where N = number of images, $k = \omega\sqrt{\mu_r \mu_o \epsilon_o}$, $r_i = \sqrt{\rho^2 + (z - z' + jb_i)^2}$ and similarly for r_i'.

D. The Air-Bridge

The CPW problem with air-bridge is shown in Fig. 6. To include the air-bridges in the formulations, the MPIE of (2) and the moment method solution of (3) must be modified as follows:

i) The boundary conditions on the air-bridge: Following the procedure outlined in Section II-A, the original CPW problem with air-bridge is transformed through duality into two full space parallel strips subproblems, with the air-bridge existing only in the upper subproblem, as shown in Fig. 7. In the upper subproblem, shown in Fig. 7(b), the air-bridge is made of a perfect magnetic conductor on which $\vec{H}_t$ vanishes. This requires a magnetic current to flow on the surface of the air-bridge that cancels the magnetic field generated by the electric currents of the strips. This effect must be employed in the modified integral equation. In addition, the magnetic currents on the air-bridges produce an electric field which couples to the electric field on the parallel strips. This effect must also be included in the modified integral equation. Therefore, the following two boundary equations must be satisfied to insure the continuity of $\vec{E}_t$ on the strips and the vanishing of $\vec{H}_t$ on the air-bridges:

$$\tfrac{1}{2}\{\hat{n}_s \times [\vec{E}_1(\vec{J}_s) - \vec{E}_2(-\vec{J}_s) + \vec{E}_M(\vec{J}_{sm})]\} = -\hat{n}_s \times \vec{E}^i$$

on the parallel strips (12)

$$\tfrac{1}{2}\{\hat{n}_b \times [\vec{H}_E(\vec{J}_s) + \vec{H}_M(\vec{J}_{sm})]\} = \underline{0}$$

on the air-bridges (13)

where $\vec{E}_1$, $\vec{E}_2$ and $\vec{E}^i$ were defined in (1). Also, following Fig. 7(b) in free space, $\vec{E}_M$ is the electric field due to a magnetic current density $\vec{J}_{sm}$ on the air-bridge and is given in (A1) of the Appendix. $\vec{H}_E$ is the magnetic field due to an electric current density $\vec{J}_s$ on the strips and is the dual of $\vec{E}_M$. $\vec{H}_M$ is the magnetic field due to a magnetic current density $\vec{J}_{sm}$ on the air-bridge. The magnetic field $\vec{H}_M$ is the dual of $\vec{E}_1$ given in (2).

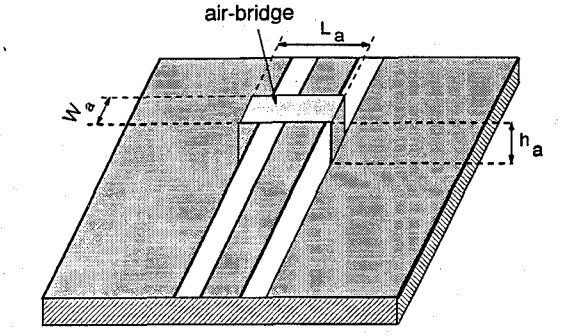

Fig. 6. A 3-D view of the coplanar waveguide with air-bridge.

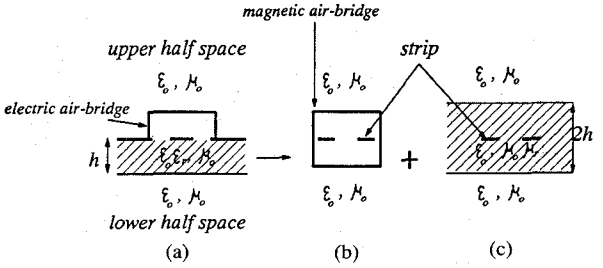

Fig. 7. Splitting the CPW problem with air-bridge into two parallel strips subproblems through duality: (a) The original CPW problem with air-bridge. (b) The upper subproblem. (c) The lower subproblem.

ii) Moment method solution of the parallel strips subproblems with air-bridges: The obtained Green's functions for $\vec{E}_M$, $\vec{H}_E$ and $\vec{H}_M$ are combined with the original integral equation (2) to yield a pair of coupled mixed potential integral equations which are solved using the moment method [13]. For this purpose, the equivalent electric currents and charges on the strips and the equivalent magnetic currents and charges on the air-bridges are expanded in terms of a finite number of pulse basis functions which satisfy the edge conditions on the strips and the air-bridges [17]. Then Galerkin's procedure is applied to yield the following matrix equation:

$$\frac{1}{2}\begin{bmatrix} [Z_1 + Z_2] & [Z^{em}] \\ [Z^{me}] & [Z^m] \end{bmatrix} \begin{bmatrix} \underline{I}^e \\ \underline{I}^m \end{bmatrix} = \begin{bmatrix} \underline{V}^e \\ \underline{V}^m \end{bmatrix} \tag{14}$$

where $\underline{I}^e$, $\underline{V}^e$, $[Z_1]$, $[Z_2]$ were defined in (3). $\underline{I}^m$ is the magnetic current on the air-bridges. $\underline{V}^m$ is the magnetic voltage excitation on the air-bridges which is zero everywhere. $[Z^m]$ is the magnetic coupling matrix and is the dual of $[Z_1]$. $[Z^{me}]$ is the magnetic-electric coupling matrix and is given in (A2) of the Appendix. $[Z^{em}]$ is the electric magnetic-coupling matrix which can be obtained from $[Z^{me}]$ using the following duality relation:

$$[Z^{em}] = -[Z^{me}]^T \tag{15}$$

where T denotes the transpose of the matrix. As in Section II-A, the half factor in (14) is due to the contribution of a half space.

It is important to mention that the matrices $[Z^{em}]$, $[Z^{me}]$ and $[Z^m]$ in (14) all represent free space couplings and can therefore be easily computed. Therefore, the air-

bridges are included in our solution of the CPW circuits using only a few additional computations.

After solving (14), the electric current on the strips is used to calculate the S-parameters following the same method mentioned in Section II-B.

III. Numerical Results and Discussions

A. The Accuracy of the Complex Image Green's Functions for CPW

Using only 4 complex images, 4 quasi-dynamic images and two surface wave terms, the complex image Green's functions gave less than 1.5% error when compared with the numerical integration of Sommerfeld integrals at different frequencies and over a large span of distances. The detailed comparison is shown in [21] and is very similar to that of the microstripline [15]. The above comparison indicates that the complex images offer a significant reduction in computation time over the numerical integration of Sommerfeld integrals.

B. The Band Reject Filter

In this section we study the CPW band reject filter shown in Fig. 8. This filter was designed by Rittweger *et al.* [10] to have no transmission at 18 GHz and good transmission at 36 GHz. The main assumption behind the design of this filter is that the CPW line behaves as a unimodal transmission line. Under this assumption each stub acts as a short circuit at $f = 18$ GHz thereby allowing no transmission between ports 1 and 2 at this frequency, while it acts as an open circuit at $f = 36$ GHz thereby allowing good transmission at this frequency.

The problem with designing the CPW filter is that the CPW shunt stubs allow both the dominant even CPW mode and the parasitic coupled (odd) slotline mode to propagate. This problem can be solved by the use of air-bridges which eliminate the coupled slotline mode by equating the potentials of the two ground planes. The locations of these air-bridges are shown in Fig. 8.

Before going into the numerical results on this filter, it is important to mention that only 87 matching points on the strips and 5 matching points on the air-bridges were used in obtaining these results. These numbers indicate a significant reduction in computation time over the FDTD method of Rittweger *et al.* [10].

C. Comparison with Rittweger's Results on the Filter Without Air-Bridges

Our results for the S-parameters of this filter without air-bridges are compared with experimental and theoretical results obtained using the FDTD method [10] as shown in Fig. 9(a) and (b). Good agreement is obtained over the whole frequency range investigated bearing in mind that both theoretical methods do not include the conductor and the dielectric losses, while the experimental results include these losses.

It is important to notice that without the air-bridges, the filter completely fails to meet the desired response of having no transmission at 18 GHz and good transmission at 36 GHz. The reason for this failure is the excitation of the coupled slotline mode in the stubs as explained.

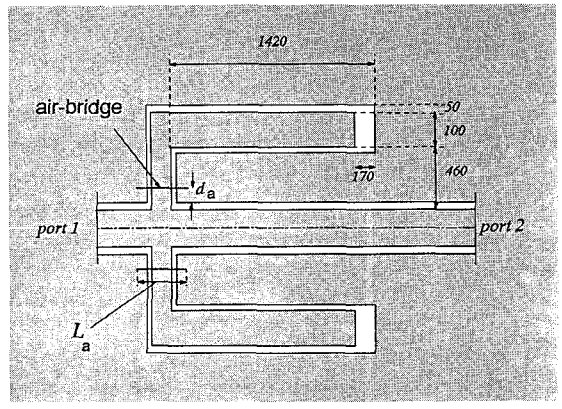

Fig. 8. The CPW band reject filter ($\epsilon_r = 9.8$, $h = 635$ μm, the dimensions are in μm).

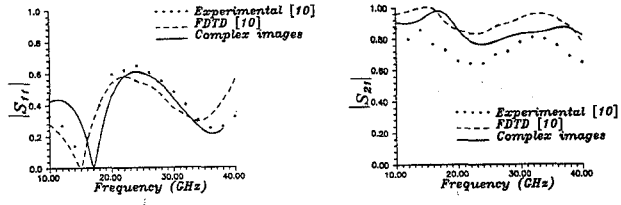

Fig. 9. The S-parameters of the CPW band reject filter, without the air-bridges, versus frequency. (a) magnitude of S_{11}. (b) magnitude of S_{21}.

D. Comparison with Rittweger's Results on the Filter With Air-Bridges

Rittweger [10] provided in his paper the locations and the lengths of the air-bridges which he used in his calculations and in the experiment. However, we had to choose, as well, the width and the height of the air-bridges based on the criterion explained later. Our results for the S-parameters of the band reject filter with air-bridges agree very well with the experimental and the theoretical results of Rittweger [10] over the whole frequency range investigated, as shown in Fig. 10(a) and (b). In addition, the filter resonant frequencies obtained agree well with the design resonant frequencies. However, the 'kink' which occurs in our results of Fig. 10(a) and (b) around 29 GHz does not agree with the 'kink' in the experimental results which occurs around 27 GHz. We suspect that this shift in the kink's position may be due to the performing of the experimental measurements with the filter inside a cavity or a package. The difference in the shapes of the two kinks may be due to the existence of conductor losses in the experimental results.

An investigation of the kink in our results revealed that it is caused by the 90° bends in the shunt stubs. This kink will, therefore, disappear when straight stubs are used. This, however, has the disadvantage of increasing the filter's size.

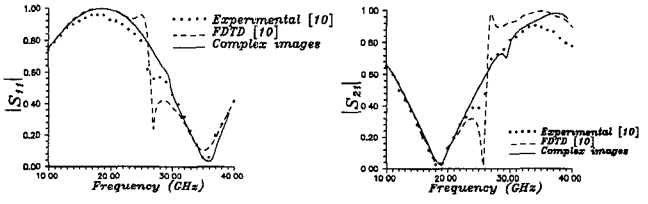

Fig. 10. The S-parameters of the CPW band reject filter, with the air-bridges, versus frequency. (a) magnitude of S_{11}. (b) magnitude of S_{21}. (h_a = 3 μm, W_a = 1 μm, l_a = 350 μm, d_a = 100 μm).

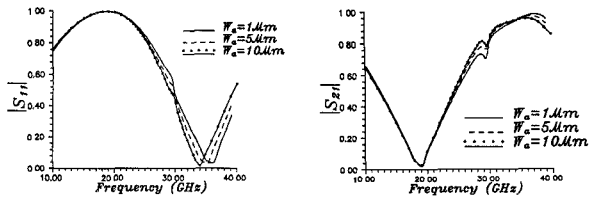

Fig. 11. The effect of the width of the airbridge (W_a) on the S-parameters of the CPW band reject filter. (a) magnitude of S_{11}. (b) magnitude of S_{21}. (h_a = 3 μm, l_a = 350 μm, d_a = 100 μm).

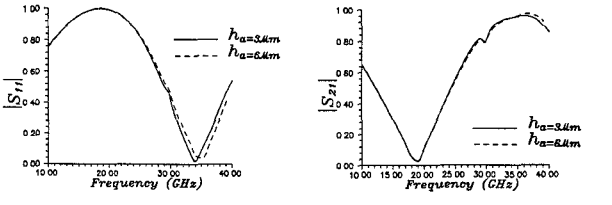

Fig. 12. The effect of the height of the airbridge (h_a) on the S-parameters of the CPW band reject filter. (a) magnitude of S_{11}. (b) magnitude of S_{21}. (W_a = 10 μm, l_a = 350 μm, d_a = 100 μm).

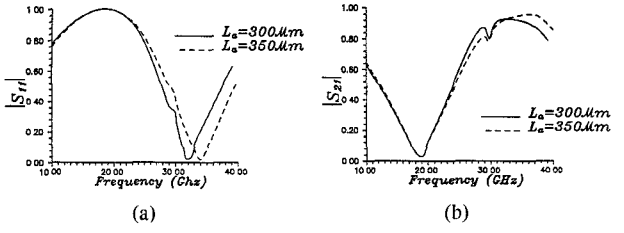

Fig. 13. The effect of the length of the airbridge (l_a) on the S-parameters of the CPW band reject filter. (a) magnitude of S_{11}. (b) magnitude of S_{21}. (W_a = 10 μm, h_a = 3 μm, d_a = 100 μm).

Therefore, it can be deduced from the previous results on the filter with bent stubs that the air-bridges play a vital role in the operation of this band reject filter. For this reason, it is expected that the locations and the dimensions of the air-bridges will affect the filter's characteristics. This is explained below:

i) The effect of the air-bridge width (W_a): Our numerical experiments on this filter show that for air-bridge widths less than 1 μm, the filter resonances agree well with the design. It is only after W_a exceeds 1 μm that the upper resonant frequency tends to shift downward, while the lower resonant frequency remains virtually unchanged, as W_a is increased. This is shown in Fig. 11(a) and (b). This behavior should be expected since an increase in the air-bridge width causes an increase in the capacitance between the air-bridge and the center strip. The effect of this capacitance becomes more significant at higher frequencies. Therefore, the stub lengths become effectively longer than their actual physical length near the upper resonant frequency, thereby shifting this resonant frequency downward.

The conclusion at this point is that, to achieve the desired response of Fig. 10, W_a should be chosen as small as practically possible, preferably around 1 μm. Below this width, the filter resonances are virtually invariant giving the correct resonant frequencies which agree with the design, while they become dependent on W_a above this limit. The very good agreement obtained in the comparisons with Rittweger [10], indicates the correctness of our choice of the width of the air-bridges.

ii) The effect of the air-bridge height (h_a): Fig. 12(a) and (b) show that an increase in the height of the air-bridges causes an increase in the upper resonant frequency of this filter while the lower resonant frequency remains virtually unchanged. The reason for this is that by increasing h_a, the capacitance between the air-bridge and the center strip decreases. This effect is more significant at higher frequencies. This will decrease the effective length of the CPW stubs near the upper resonant frequency, thereby shifting this frequency upward.

In our comparisons with Rittweger [10], we chose h_a = 3 μm which is a typical height for these air-bridges.

iii) The effect of the air-bridge length (L_a): Our numerical experiments show that the length of the air-bridges, as defined in Fig. 6, significantly affects the upper resonant frequency of the band reject filter, such that this resonant frequency increases with increasing L_a as shown in Fig. 13(a) and (b). The reason for this is that by increasing the length of the air-bridges, their inductances increase, thereby decreasing the net capacitive reactance between the center strip and the ground plane at the air-bridge locations. This effect is more significant at higher frequencies at which each stub becomes effectively shorter than its actual length. This will shift the upper resonant frequency of the filter upward while virtually not changing the lower resonant frequency. It is important to note that the significance of the length of the air-bridges on the filter resonances was also reported by Rittweger [10].

iv) The effect of the air-bridge location (d_a): It was numerically found that for values of d_a less than 100 μm, the filter's resonant frequencies agree well with the design resonant frequencies. Above this limit, the lower and upper resonant frequencies tend to shift upward as d_a is increased (i.e. as the air-bridges move farther away from the CPW line). This is shown in Fig. 14(a) and (b). This effect was also confirmed by Rittweger [10]. The reason for this behavior is that by making (d_a) larger, the coupled slotline mode is allowed to propagate for a longer distance along each stub before being eliminated by the air-bridges. Since the coupled slotline mode propagates at a higher speed than the dominant CPW mode, therefore, each stub

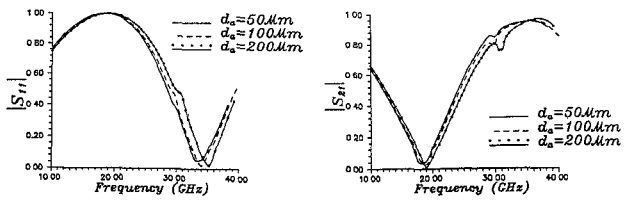

Fig. 14. The effect of the location of the airbridge (d_a) on the S-parameters of the CPW band reject filter. (a) magnitude of S_{11}. (b) magnitude of S_{21} (W_a = 10 μm, h_a = 3 μm, l_a = 350 μm).

becomes effectively shorter because of the coupled slotline mode. This causes an upward shift in the resonant frequencies of the filter as (d_a) is increased. The implication is that it is better to choose (d_a) as small as possible, preferably below 100 μm, to insure that the resonant frequencies of the filter occur where they should. This conclusion was also reached by Rittweger [10]. It is also important to note that the curves were calculated for wide air-bridges (W_a = 10 μm). This causes a small downward shift in the upper resonant frequency from that of Fig. 10(a) and (b).

IV. Conclusions

A new technique for solving general CPW circuits including the air-bridges is proposed to solve the problem of coupled slotline mode excitation in nonsymmetric CPW circuits. This technique generalizes the integral equation technique to solve nonplanar structures which contain hybrid electric and magnetic currents, such as the CPW with air-bridges. This generalized integral equation technique, combined with the moment method which uses the efficient multi-pipes [20] and with the accurate and efficient complex image Green's functions, provides a powerful, accurate and numerically efficient method for solving CPW circuits and air-bridges. In particular, the complex image technique avoids the time consuming numerical integration of Sommerfeld integrals. In addition, the resultant Green's functions consist of only 4 quasi-dynamic images, 4 complex images and 2 surface wave terms. This constitutes at least a 10 fold reduction in computation time as compared to the numerical integration with less than 1.5% error.

The proposed method is tested on a CPW band reject filter previously solved using the FDTD method. Our method uses only 87 matching points on the strips and 5 matching points on the air-bridges (resulting in 3 minutes for each frequency on a 33 MHz 80386 PC) to achieve the same kind of accuracy obtained using the FDTD method which is time consuming and requires a large computer memory. Therefore, the proposed method offers a significant reduction in computation time and memory without sacrificing the accuracy.

Our method is then applied to analyze the behavior of the CPW band reject filter and the effects of the air-bridges' locations and dimensions on this behavior. The conclusion from this analysis is that the existence of the air-bridges is crucial to the filter and that the filter's characteristics significantly depend on the dimensions and locations of these air-bridges. Therefore, by merely adjusting the air-bridge parameters, it is possible to control the filter's characteristics.

Appendix
The Electric and Magnetic Couplings in the Air-Bridge Subproblem

The electric field due to a magnetic current density $\vec{J}_{sm}$ in free space is given by

$$\vec{E}_M = -\frac{1}{4\pi}\int_{S_m^m} \frac{e^{-jk_o r}}{r}\left[jk_o + \frac{1}{r}\right](\vec{J}_{sm} \times \hat{r})\, dS_m^m \quad \text{(A1)}$$

where $\hat{r}$ is a unit vector pointing from the magnetic source point to the field point. k_o is the free space propagation constant, and S_m^m is the surface area of the air-bridge segment m. The magnetic voltage on the air-bridge segment m due to a unit electric current on the strip segment n is given by:

$$Z_{mn}^{me} = \frac{-1}{4\pi}\int_{S_n^e}\int_{S_m^m} f_n f_m \frac{e^{-jk_o r_{me}}}{r_{me}}\left[jk_o + \frac{1}{r_{me}}\right](\hat{a}_e \times \hat{r}_{me}) \cdot \hat{a}_m\, ds_m^m\, ds_n^e \quad \text{(A2)}$$

where $\hat{a}_e$, $\hat{a}_m$ are unit vectors pointing in the direction of the electric and magnetic currents, respectively. f_n, f_m are the basis functions of electric segment n and magnetic segment m, respectively. These basis functions were explained in Section II-D. $\hat{r}_{me}$ is a unit vector pointing from the electric source point to the magnetic field point, and S_n^e is the surface area of the strip segment n. Equation (A2) is integrated analytically to reduce the computation time.

Acknowledgment

The authors would like to thank Prof. G. E. Howard and Dr. J. J. Yang for many interesting discussions and helpful suggestions.

References

[1] R. W. Jackson, "Consideration in the use of coplanar waveguide for millimeter wave integrated circuits," *IEEE Trans. Microwave Theory Tech.*, vol. MTT-34, pp. 1450-1456, Dec. 1986.

[2] A. A. Omar and Y. L. Chow, "An accurate 3-D solution of coplanar waveguides by the duality principle of dipoles and slots," in *IEEE AP-S Dig.*, 1991, pp. 878-881.

[3] M. Riaziat *et al.*, "Coplanar waveguides used in 2-18 GHz distributed amplifer," *IEEE MTT-S Dig.*, June 1986, pp. 337-338.

[4] R. H. Jansen, "Hybrid mode analysis of end effects of planar microwave and millimeter wave transmission lines," *Proc. Inst. Elec. Eng.*, vol. 128, pt. H, no. 2, pp. 77-85, Apr. 1981.

[5] N. I. Dib and P. B. Katehi, "Modeling of shielded CPW discontinuities using the space domain integral equation method (SDIE)," *J. Electromagn. Waves Appl.*, vol. 5, no. 4-5, pp. 503-523, 1991.

[6] M. Drissi, V. F. Hanna, and J. Citerne, "Analysis of coplanar waveguide radiating end effects using the integral equation technique," *IEEE Trans. Microwave Theory Tech.*, vol. 39, pp. 112-116, Jan. 1991.

[7] M. Rittweger, N. H. L. Koster, S. Koßlowski, R. Bertenburg, S. Heinen, and I. Wolff, "Full-wave analysis of a modified coplanar airbridge T-junction," in *21st European Microwave Conf. Proc.*, pp. 993-998, 1991.

[8] N. I. Dib, P. B. Katehi and G. E. Ponchak, "Analysis of shielded CPW discontinuities with air-bridges," in *IEEE MTT-S Dig.*, 1991, pp. 469–472.
[9] R. Bromme and R. H. Jansen, "Systematic investigation of coplanar waveguide MIC/MMIC structures using a modified strip/slot 3D electromagnetic simulator," in *IEEE MTT-S Dig.* 1991, pp. 1081–1084.
[10] M. Rittweger, M. Abdo, and I. Wolff, "Full-wave analysis of coplanar discontinuities considering three dimensional bond wires," in *IEEE MTT-S Dig.*, 1991, pp. 465–468.
[11] K. Beilenhoff, W. Heinrich, and H. L. Hartnagel, "The scattering behavior of air bridges in coplanar MMICs," in *21st European Microwave Conf. Proc.*, 1991, pp. 1131–1135.
[12] J. R. Mosig, "Integral equation technique," in T. Itoh, Ed., *Numerical Techniques for Microwave and Millimeter-Wave Passive Structures.* New York: Wiley, 1989, pp. 133–207.
[13] R. F. Harrington, *Field Computation by Moment Methods.* Malabar, FL, Robert E. Krieger, 1968, pp. 62–81.
[14] P. L. Sullivan and D. H. Schaubert, "Analysis of an aperture coupled microstrip antenna," *IEEE Trans. Antennas Propagat.*, vol. AP-34, pp. 977–984, 1986.
[15] Y. L. Chow, J. J. Yang, D. G. Fang, and G. E. Howard, "A closed form spatial Green's function for thick microstrip substrate," *IEEE Trans. Microwave Theory Tech.*, vol. 39, no. 3, pp. 588–593, Mar. 1991.
[16] E. C. Jordan and K. G. Balmain, *Electromagnetic Waves and Radiating Systems.* Englewood Cliffs, NJ: Prentice-Hall, 1968, pp. 513–519.
[17] R. E. Collin, *Field Theory of Guided Waves.* New York: McGraw Hill, 1991, pp. 23–26.
[18] Y. L. Chow, G. E. Howard, and M. G. Stubbs, "The Watmic, A software that treats microwave integrated circuits like linear antennas," *ANTEM'88 Conf. Proc.*, Aug. 1988, Winnipeg, MB, Canada.
[19] Y. L. Chow and G. E. Howard, "The short circuit and load for the moment solution of a microstripline," in *1990 URSI Radio Science Meeting*, Dallas, TX.
[20] G. E. Howard, J. J. Yang, and Y. L. Chow, "A multi-pipe model of general strip transmission lines for rapid convergence of integral equation singularities," *IEEE Trans. Microwave Theory Tech*, vol. 40, no. 4, Apr. 1992.
[21] A. A. Omar and Y. L. Chow, "The complex image Green's functions for coplanar waveguides," to appear in *IEEE AP-S Digest* in July 1992.
[22] Y. L. Chow, "An approximate dynamic Green's function in three dimensions for finite length microstripline," *IEEE Trans. Microwave Theory Tech.*, vol. MTT-28, no. 4, pp. 393–397, Apr. 1980.
[23] R. W. Hamming, *Numerical Methods for Scientists and Engineers.* New York: Dover 1973, pp. 620–622.
[24] J. A. Stratton, *Electromagnetic Theory.* New York: McGraw-Hill, 1941, pp. 576, eq. 17.

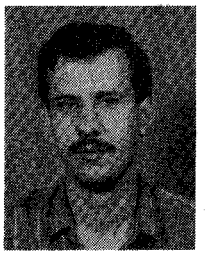

Amjad A. Omar was born in Kuwait, on December 15, 1963. He received the B.Sc. and M.Sc. Degrees from Kuwait University, Kuwait, in 1985 and 1988, respectively. Currently he is working towards the Ph.D. degree at the University of Waterloo, Waterloo, ON, Canada.

From 1985 to 1989 he was a Research and a Teaching Assistant with the Department of Electrical and Computer Engineering, Kuwait University. Since 1989 he has been a Research and a Teaching Assistant with the Department of Electrical and Computer Engineering, University of Waterloo. His current research interests are in the numerical solution of microwave and millimeter-wave integrated circuits.

Y. Leonard Chow (S'60–M'65) received the B.Eng. degree in 1960 from McGill University, Montreal, Que., Canada, and the M.A.Sc. and Ph.D. degrees in 1961 and 1965 from the University of Toronto, Toronto, ON, Canada.

From 1964 to 1966, he worked for the National Radio Astronomy Observatory, Charlottesville, VA. As a consequence, in 1974 he designed the array configuration for the Very Large Antenna Array, which comprises 27 85-ft parabolic reflectors and is located in Socorro, NM. In 1966 he joined the University of Waterloo, Waterloo, ON, Canada, and became a Professor in the Department of Electrical and Computer Engineering. Presently his research deals with the numerical simulation of field effects. The field effects range from high-voltage dc fields to antennas and to fields of microwave integrated circuits, both linear and nonlinear. In the microwave integrated circuit area, he is a consultant to both the Communication Research Center, Canada, and EEsof Inc., California. He is the principal author of the field-theory-based MIC package EMsim. of EEsof Inc.